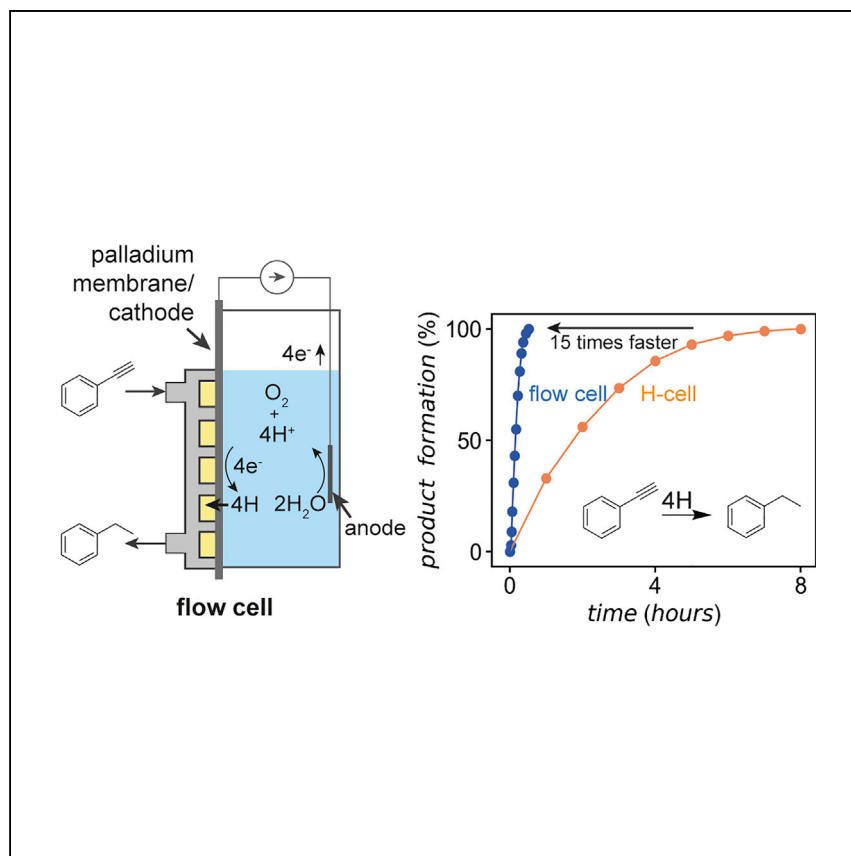


Article

Hydrogenation without H₂ Using a Palladium Membrane Flow Cell



Electrocatalytic palladium membrane reactors hydrogenate organic molecules using water and electricity as the only inputs. In this work, Jansonius et al. report a flow cell architecture that enables 15-fold faster reaction rates with twice the current efficiency of a batch cell.

Ryan P. Jansonius, Aiko Kurimoto, Antonio M. Marelli, Aoxue Huang, Rebecca S. Sherbo, Curtis P. Berlinguette

cberling@chem.ubc.ca

HIGHLIGHTS

Electrocatalytic palladium membrane reactors enable hydrogenation without H₂ gas

Flow cell design increases reaction rates 15-fold

Reaction rate and selectivity can be controlled by the applied electrochemical current

Jansonius et al., Cell Reports Physical Science 1, 100105

July 22, 2020 © 2020 The Authors.

<https://doi.org/10.1016/j.xcrp.2020.100105>



Article

Hydrogenation without H₂ Using
a Palladium Membrane Flow Cell

Ryan P. Jansonius,¹ Aiko Kurimoto,¹ Antonio M. Marelli,¹ Aoxue Huang,¹ Rebecca S. Sherbo,¹
and Curtis P. Berlinguette^{1,2,3,4,5,6,*}

SUMMARY

Electrocatalytic palladium membrane reactors (ePMRs) use electricity to hydrogenate organic molecules at ambient temperature and pressure. These benign reaction conditions position ePMRs as a sustainable alternative to thermochemical hydrogenation, which requires high-temperature and high-pressure reaction conditions. However, ePMRs suffer from slow reaction rates and a limited understanding of the factors that govern reaction performance in these devices. In this work, we report the design and validation of an ePMR flow cell. This flow cell increases reaction rates 15-fold and current efficiencies by 30% relative to H-cell reactors. We use this device to reveal that the hydrogen content in the palladium membrane governs the speed and selectivity of hydrogenation reactions, while the amount of hydrogen gas evolved at the palladium surface is deterministic of current efficiency. We contend that this flow cell, which enables hydrogenation without hydrogen gas, is an important step for translating ePMRs into practice.

INTRODUCTION

Using renewable electricity to drive chemical transformations provides a route to sustainable chemical manufacture.¹ This situation has motivated the development of electrochemical methods to replace conventionally thermally driven reactions (e.g., ammonia,² hydrocarbon,³ hydrogen production⁴). Hydrogenation reactions have received far less attention, yet electrification of this process could have a meaningful impact on the production of fine chemicals,^{5,6} food,⁷ and biofuels.⁸ The electrocatalytic palladium membrane reactor (ePMR) is a technology that uses electricity to facilitate the hydrogenation of organic molecules under ambient conditions using electrochemically reduced protons as the hydrogen source.^{9–13} ePMRs present the opportunity to use hydrogen while circumventing the use of H₂ gas, which is challenging to store and transport. We demonstrate herein an ePMR flow cell architecture that enables efficient electrically driven hydrogenation and shows a possible pathway for scaling this unique reactor design.

The enabling feature of an ePMR is that a thin palladium membrane is simultaneously used as (1) a cathode to electrocatalytically reduce protons to reactive hydrogen, (2) a hydrogen-selective membrane to transport reactive hydrogen to the reaction site, and (3) a chemical hydrogenation catalyst. In this reactor, protons produced from the oxygen evolution reaction (OER),^{9,12,13} or the oxidation of an organic species at a platinum anode,¹¹ are reduced at the palladium membrane surface. Hydrogen atoms adsorbed to the palladium surface subsequently absorb into interstitial sites in the fcc palladium lattice,¹⁴ permeate across the membrane to the opposite

¹Department of Chemistry, The University of British Columbia, 2036 Main Mall, Vancouver, BC V6T 1Z1, Canada

²Stewart Blusson Quantum Matter Institute, The University of British Columbia, 2355 East Mall, Vancouver, BC V6T 1Z4, Canada

³Department of Chemical and Biological Engineering, The University of British Columbia, 2360 East Mall, Vancouver, BC V6T 1Z3, Canada

⁴Canadian Institute for Advanced Research (CIFAR), 661 University Avenue, Toronto, ON M5G 1M1, Canada

⁵Twitter: @cpbCleanEnergy

⁶Lead Contact

*Correspondence: cberling@chem.ubc.ca
<https://doi.org/10.1016/j.xcrp.2020.100105>



surface of the foil, and react with an unsaturated organic feedstock to produce the saturated (or partially saturated) adduct.^{9,11}

This technology leverages key attributes of both electrocatalytic hydrogenation⁹ and thermally driven palladium membrane hydrogenation.¹⁵ Harvesting H atoms electrolytically enables high hydrogen fugacities to be accessed without a pressure vessel,¹⁶ and using palladium as a hydrogen-selective membrane between the electrolysis chamber and the hydrogenation chamber enables the electrochemistry to be physically separated from the hydrogenation reaction, circumventing the challenging separation of organic products from the electrolyte.^{9,17} In spite of the advantages of ePMRs over these competing technologies, there are currently few reports of these systems.^{9–13,18–22} Studies to date have demonstrated the hydrogenation of carbon dioxide,¹⁹ alkynes,^{9,11,12} aldehydes, and imines (data not shown). While these studies highlight the potential of this technology in applications in organic synthesis, commodity chemical manufacture, or CO₂ valorization, ePMRs are presently hindered by low conversion rates and a limited understanding of the factors that mediate hydrogenation performance (i.e., reaction rate, selectivity, and current efficiency) in these devices.

Previous ePMR studies have been carried out in H-cells (Figure 1A), a reactor architecture convenient for proof-of-concept research,³ but not relevant for commercial applications. We addressed this technological gap by constructing an ePMR flow cell. This electrochemical flow cell was designed to deliver an organic feedstock to the catalyst surface through a flow field (Figure 1B). Our approach was informed by the development of analogous flow cell systems such as hydrogen fuel cells,²³ and water and CO₂ electrolyzers.³ Given that flow cell architectures have been shown to drastically improve reaction performance and are a key step in commercial scale-up,^{3,24,25} we elected to address reactor design limitations early in ePMR development.

We demonstrate herein that an ePMR flow cell enables faster, more selective, and higher efficiency hydrogenation. We validate this flow cell by studying the hydrogenation of phenylacetylene (PA) as a simple model reaction and tracking the factors that determine reaction rate, selectivity, and efficiency. Through reactor design alone (i.e., flowing the organic reactant to the catalyst surface and decreasing the solution resistance in the electrolysis chamber), we can achieve 15-fold higher hydrogenation rates than can be accessed in an H-cell at a similar applied voltage. This reactor also reveals unique insights into reaction performance. Hydrogenation is determined to proceed following the well-established sequential hydrogenation mechanism²⁶ as well as through a direct hydrogenation pathway in which the alkyne is directly converted to the alkane adduct in a single step.²⁷ Hydrogen content in the membrane is found to be deterministic of the hydrogenation rate, in which more absorbed hydrogen leads to faster, albeit less selective, conversion. These findings highlight that both reactor design and palladium membrane properties play a role in hydrogenation performance, providing reactor and palladium membrane design principles to guide ePMR technologies toward applications in synthesis and commodity chemical manufacturing.

RESULTS AND DISCUSSION

Design of an Electrochemical Palladium Membrane Flow Cell

For the first stage of this study, we designed and constructed a 3-chamber ePMR flow cell (Figure 1C). This device includes (1) separate electrochemical

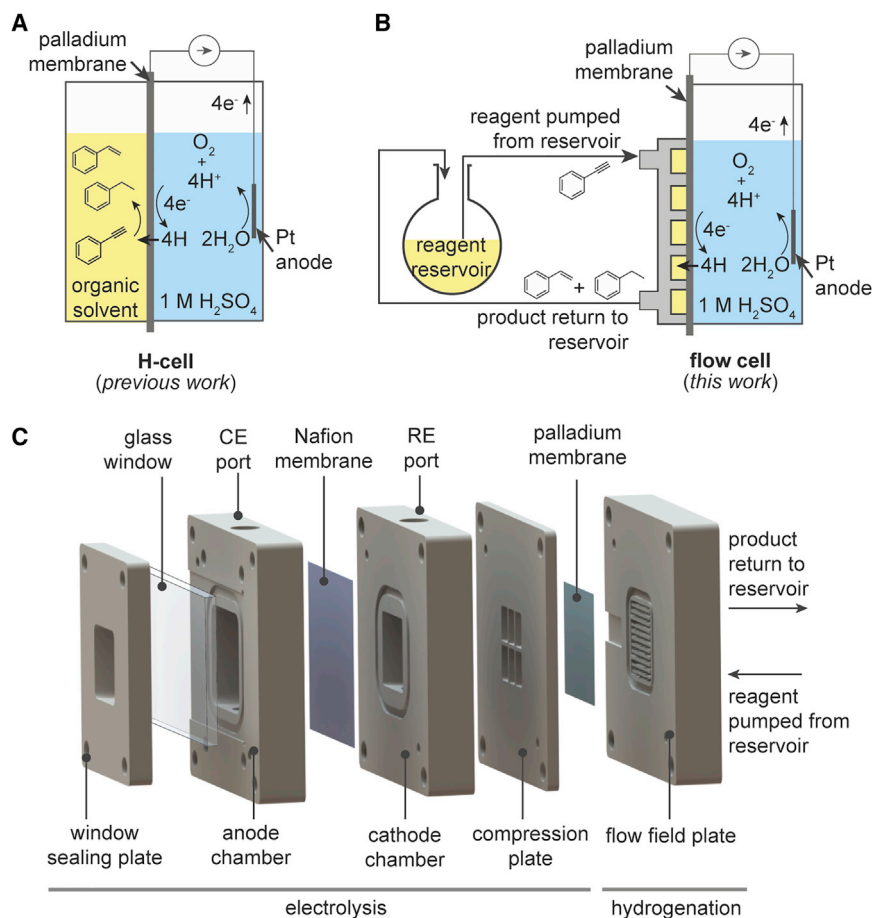


Figure 1. Electrocatalytic Palladium Membrane Reactor Architectures

(A and B) Illustrations of (A) the 2-compartment H-cell reactor architecture used to date for electrocatalytic palladium membrane hydrogenation reactions (see Figure S3 for an image of the H-cell setup)^{9,11} and (B) the ePMR flow cell architecture reported here, wherein the organic reagent is delivered to the catalyst surface through a flow field plate.

(C) Rendering of the ePMR flow cell, which includes electrolysis and hydrogenation compartments partitioned by a palladium membrane. The electrolysis compartment houses a 3-electrode electrochemical setup, and the hydrogenation compartment includes a flow field plate with a triple serpentine flow pattern for efficient reagent delivery (see Figure S1 for an image of the complete setup and Figure S2 for an image of each component).

compartments to contain the platinum anode and the reference electrode (RE) and palladium membrane and (2) a hydrogenation flow field plate with a 2×2 cm triple serpentine flow pattern and 1×1 mm flow channels. The anode and cathode chambers were separated by a Nafion membrane to isolate oxidative electrochemistry from proton reduction at the palladium cathode (3×3 cm),¹¹ which was held securely against the flow field by a compression plate. O-rings (Viton, square cross-section) were used to reliably seal the intercompartmental interfaces. This sealing strategy enabled more efficient use of the palladium foil, with a 3.7-fold increase in the active area of palladium (from 1.2 cm^2 to 4 cm^2) compared to our previously reported H-cell configuration despite only requiring a mere 1.4 times larger palladium foil. A high surface area palladium black catalyst was electrodeposited on the hydrogenation side of the palladium membrane to increase the reaction rate, according to previously reported procedures (see Figures S5 and S6 for characterization).¹¹

To conduct hydrogenation experiments in the flow cell, the cathode and anode compartments were both filled with 8 mL 1 M H₂SO₄ electrolyte, then a Ag/AgCl RE and platinum mesh counter electrode (CE) were inserted through the dedicated ports in each half of the electrolysis compartment. For each hydrogenation reaction, a fresh solution of PA (25 mL, 0.1 M in dichloromethane [DCM]) contained in a 50-mL reservoir, was continuously recirculated through the hydrogenation flow field at a rate of 20 mL/min using a peristaltic pump. Water electrolysis was driven galvanostatically at a current of 10, 50, 100, 250, or 400 mA/cm², and reaction progress was monitored by quantifying the amounts of PA, styrene (ST) and ethylbenzene (EB) in 20-μL aliquots taken from the reagent reservoir using gas chromatography-mass spectrometry (GC-MS). These data were used to generate concentration versus time plots (Figures 2A, S9, and S16A), which were subsequently analyzed to determine reaction rate, selectivity, and current efficiency.

A primary goal of this reactor design was to enable faster and more efficient conversion than can be achieved in an H-cell. There are 4 major steps that must proceed for hydrogenation to occur in these devices: (1) proton reduction at the cathode surface, (2) hydrogen permeation through the palladium membrane, (3) diffusion of an organic substrate to the surface of the membrane, and (4) hydrogen addition across the unsaturations of the organic substrate. While there has (to date) been very little study of the factors that determine reaction performance in ePMRs, previous studies have shown that improving diffusion kinetics by depositing a rough, high surface area catalyst on the hydrogenation surface of the membrane substantially increases the reaction rate.^{11,19} This observation suggests that the reaction performance may be increased by further improving diffusion kinetics, motivating our use of a flow field at the hydrogenation surface of the membrane in the ePMR flow cell.

We also redesigned the electrolysis chamber to enable higher current densities (also known to have a marked effect on reaction performance^{11,12}). Previous studies have shown that driving higher electrolysis currents (i.e., increasing the rate of proton reduction) forces more hydrogen through the membrane and results in faster, albeit less selective, hydrogenation. Minimizing the interelectrode distance (i.e., the distance between the palladium cathode and platinum anode) decreased voltage losses from electrolyte resistance and enabled electrolysis at substantially higher current densities for a similar applied voltage; 5.6 V was required to drive 100 mA/cm² electrolysis in the H-cell and a 5.8-V bias facilitated 400 mA/cm² electrolysis in the flow cell (Figure S7). We note that additional measures could be taken to decrease cell voltage to enable even higher current densities, including increasing the anode surface area or implementing a membrane electrode assembly design similar to analogous electrochemical flow cells (e.g., hydrogen fuel cells, water electrolyzers, CO₂ electrolyzers).³

Benchmarking Hydrogenation Reaction Performance in the Flow Cell

With this flow cell in hand, we set out to validate our design approach by conducting a series of experiments to benchmark reaction performance in this device. Our first set of experiments compared hydrogenation performance (i.e., reaction rate, selectivity, and current efficiency) between the flow cell and an H-cell setup. A hydrogenation reaction was carried out in each cell architecture at a fixed current density of 100 mA/cm² using 25 mL 0.1 M PA in DCM as the reactant and 1 M H₂SO₄ as the electrolyte. The H-cell was assembled according to our previously reported procedures,^{9–11} using a (2.5 × 2.5 cm) palladium foil to separate the stirred hydrogenation and electrolysis chambers. To enable a direct comparison of reaction performance metrics between each cell architecture, we used Kapton film to mask the surface

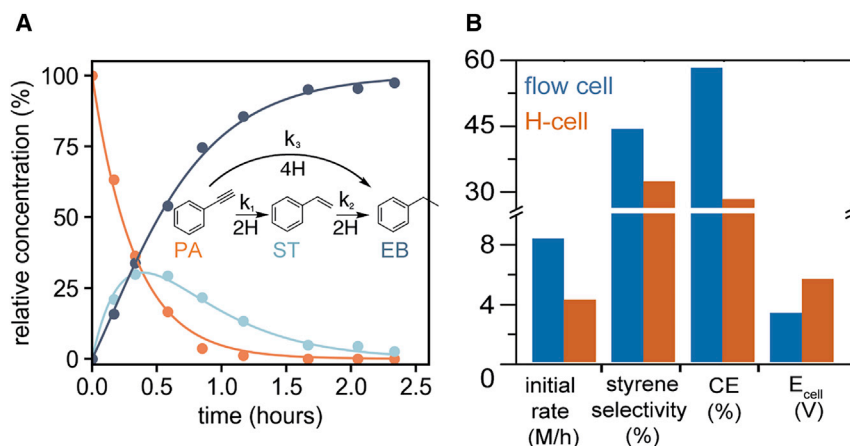


Figure 2. Comparison of Hydrogenation Performance in an ePMR H-Cell and Flow Cell

(A) Concentration profile of a hydrogenation reaction carried out at 250 mA/cm^2 in the ePMR flow cell. The inset scheme shows that hydrogenation of phenylacetylene (PA) may proceed via a styrene (ST) intermediate or directly to ethylbenzene (EB) in a single step. Kinetic fits (indicated by solid lines) were determined by finding the best fit for Equations S4–S6 to experimental data (see [Note S1](#)).

(B) Bar chart comparing reaction performance in an H-cell (see [Figure S4](#) for raw data) and a flow cell with an identical palladium surface area using 4 reaction performance metrics: initial reaction rate, maximum styrene concentration, current efficiency (CE), and cell voltage (E_{cell}) at 100 mA/cm^2 . The flow architecture enables higher performance on every metric than does the H-cell.

of the palladium foil used in the flow cell so that the active area of the catalyst was equal in both setups (i.e., 1.2 cm^2).

This benchmarking experiment revealed that the flow cell outperforms the H-cell on every key performance metric ([Figure 2B](#)). The initial reaction rate increased 2-fold when the reaction was run in flow compared to the static H-cell. Selectivity for ST production was also found to be slightly higher in the flow cell (43% maximum styrene concentration, cf. 32% in the H-cell), and current efficiency was found to be 2-fold higher in the flow cell than in the H-cell. Flow rate also adjusted the reaction rate, with higher flow rates driving faster hydrogenation (i.e., 0.18 M/h at a flow rate of 10 mL/min and 0.26 M/h at 40 mL/min ; [Figure S8](#)). Cell design modifications also facilitated a substantial decrease in cell voltage (from 5.6 to 3.3 V) required to drive a 100-mA/cm^2 electrolysis current ([Figure S7](#)). These results show how this reactor design alone can be used to achieve remarkable performance gains without more complicated catalyst or material modifications.

Our benchmarking experiments also aimed to show that electrolysis current density can be used as an easily accessible variable to control reaction rate, selectivity, and current efficiency. We again performed hydrogenation of PA in the flow cell, but used the entire 4 cm^2 surface area of the foil and conducted galvanostatic electrolysis at 10 , 50 , 100 , 250 , and 400 mA/cm^2 . The reaction rate, selectivity, and current efficiency were quantified for each reaction ([Figure 3](#)). We found that higher current densities drive faster reaction rates ([Figure 3A](#)) and higher selectivity for the EB adduct ([Figure 3B](#)), albeit at the cost of lower current efficiencies ([Figure 3C](#)). These experiments collectively served to verify that electrochemical control of the reaction rate, selectivity, and efficiency^{9,11,12} was not sacrificed by modifying the reactor architecture. Our results also highlight the marked effect that current density has on reaction performance, with the ability to modulate the reaction rate 19-fold, the

selectivity 5-fold, and the current efficiency 3-fold by adjusting the electrolysis current between 10 and 400 mA/cm².

As a final validation experiment, we demonstrated that the reaction scale can be easily increased by simply changing the size of the chemical reservoir. We hydrogenated a 200-mL, 0.2-M (40 mmol, 3.8 g, in DCM) solution of PA at 100 mA/cm², which required 24 h of continuous electrolysis to consume the starting material (see [Figure S10](#)). Selectivity for the ST intermediate was roughly 2-fold higher than the reaction conducted using a 0.1-M PA solution, showing that concentration is an additional variable for manipulating reaction selectivity. This experiment also demonstrates that the palladium membrane is sufficiently durable for extended operation.

Palladium Membrane Properties Determine Hydrogenation Reaction Performance

We next set out to understand the processes that govern the hydrogenation rate, selectivity, and current efficiency in an ePMR using a simple kinetic model. This model (described in detail in the [Supplemental Information](#)) used a custom Python script to extract the effective rate constants (i.e., the rate constant multiplied by [H]; denoted as k_x')⁹ for each step of the hydrogenation reaction by fitting a system of differential equations to reaction concentration profiles. The reaction was found to be first order in PA and ST for current densities >10 mA/cm² and 0-order in the organic reactants for the lowest current density tested ([Figures S11–S15](#); [Table S1](#); [Note S1](#)), suggesting that the reaction is rate limited by hydrogen delivery at 10 mA/cm² and hindered by either hydrogen addition to the substrate or substrate diffusion to the catalyst surface at higher current densities (≥ 50 mA/cm²). This assertion is supported by current efficiency data ([Figure 3C](#)), showing that at 10 mA/cm², nearly all of the hydrogen produced is consumed by the hydrogenation reaction, and at currents ≥ 50 mA/cm², excess hydrogen is produced and evolved as H₂(g) by-product.

Horiuti and Polanyi^{26,28} originally proposed a sequential hydrogenation mechanism that proceeds through a partially hydrogenated alkene (i.e., ST) intermediate, which can either desorb from the metal surface or react further to form the alkane (i.e., EB) product.^{27,29} We found that adding a direct hydrogenation pathway,^{27,30} wherein PA is converted to EB in a single step ([Figure 2A](#), inset scheme), provided a higher goodness-of-fit at every current density tested ([Figures S17–S20](#); [Table S2](#); [Note S2](#)). A key outcome of this model is that current density appears to gate the preference for the sequential or direct hydrogenation pathways. The effective rate constant for the direct hydrogenation pathway (k_3') is nearly 100-fold larger relative to the sequential pathway (k_1' , k_2') at 400 mA/cm² than at 10 mA/cm² (see [Table S3](#)). High current densities (≥ 100 mA/cm²) therefore result in low selectivity for the ST intermediate because ST is simply hydrogenated to EB before desorption can occur.

Next, we turned our attention to the palladium membrane to understand the dramatic influence that electrochemical current exerts over the hydrogenation reaction performance. We experimentally resolved how reaction performance correlates to (1) the hydrogen content of the palladium membrane and (2) the amount of hydrogen that evolves from each side of the membrane. A coulometry method we developed³¹ was used to conduct *ex situ* measurements of the palladium membrane hydrogen content (expressed as the H:Pd ratio) at a range of potentials between 0 and –1.0 V versus the reversible hydrogen electrode (RHE; [Figure 4A](#)). We used

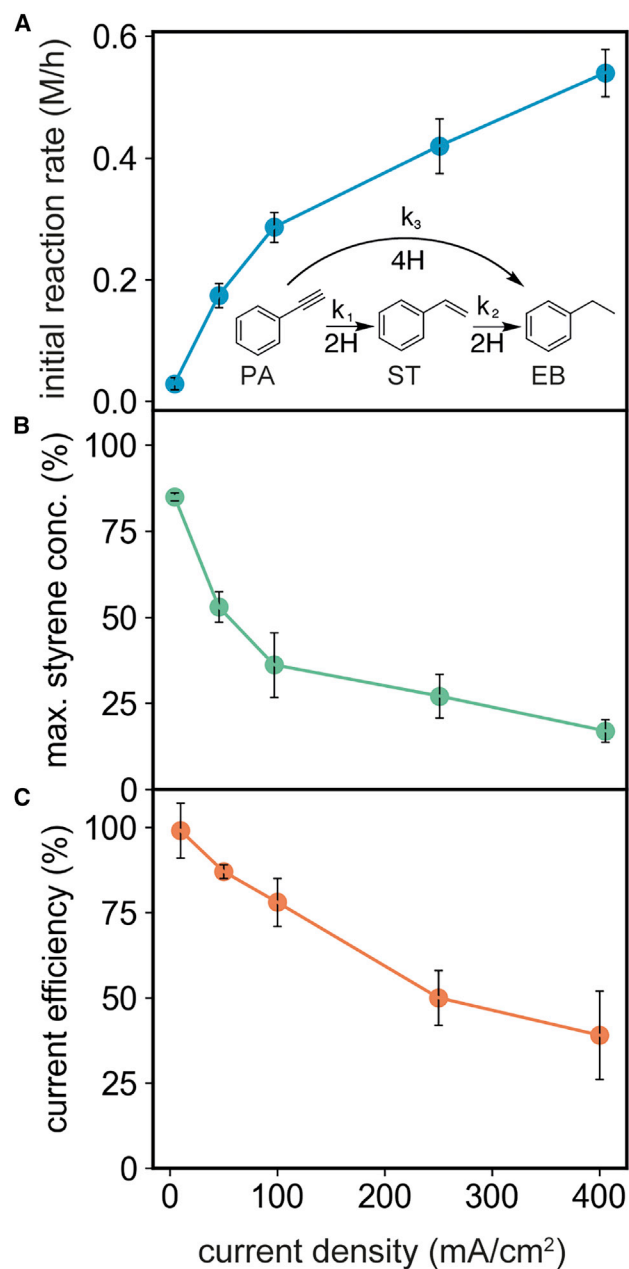


Figure 3. Current Density Influences Reaction Performance in a Flow Cell

Plots showing the effect of current density on (A) the initial rate of PA hydrogenation to styrene and EB (reaction scheme inset), (B) maximum styrene concentration, and (C) current efficiency, as a function of current density in an ePMR flow cell. Current density increases the hydrogenation reaction rate while concurrently decreasing selectivity and current efficiency. Each data point represents the average value from at least 3 reactions, with error bars representing ± 1 standard deviation of the mean value.

these data to calculate the palladium membrane hydrogen content at each hydrogenation current density by substituting the average cathode potentials at 10, 50, 100, 250, and 400 mA/cm² into the equation of the fit (Figure 4B, also see Equation S20 and Figure S23).

These experiments clearly show that hydrogen content in the membrane affects reaction rate and selectivity; a lower concentration of hydrogen in the membrane leads to slower but more selective hydrogenation (Figures 4C and 4D, respectively). This finding is qualitatively consistent with previous studies showing that catalytic promoters dissolved in the palladium catalyst (e.g., carbon,^{32,33} silver^{34,35}) decrease hydrogen loading, and resultantly increase the selectivity for the alkene intermediate (but at the cost of a decreased reaction rate).^{34–36} We show that a powerful feature of the ePMR system is that reaction rate and selectivity can be modulated by simply adjusting the current density, thus circumventing the need for exotic catalyst designs.^{37,38} Electrochemical control of the H: Pd ratio enabled us to use this device to study the influence of absorbed hydrogen on reaction performance, in which previous studies of hydrogenation catalysts have required more elaborate high-vacuum setups.^{33,38,39}

Finally, we investigated how current density affects current efficiency by using *in situ* mass spectrometry to measure the amount of hydrogen evolved from each side of the palladium membrane during electrolysis. An atmospheric pressure-mass spectrometer (atm-MS) was connected to the organic reagent reservoir filled with 25 mL DCM (Figure 5A). Electrolysis was conducted for >1,000 s at a current density of 10, 50, 100, 250, and 400 mA/cm² while DCM was continuously recirculated through the hydrogenation flow field. The amount of hydrogen that permeated through the membrane was measured by monitoring the mass-to-charge ratio for hydrogen ($m/z = 2$) with the atmospheric pressure-mass spectrometer. The hydrogen permeation rate (which is proportional to the ion current) measured at each side of the membrane increased with current density (see Figure 5B for the reagent reservoir measurement; see Figure S24 for the hydrogen measured in the electrolysis chamber). The current efficiency tracked linearly with permeated hydrogen (Figure 5C), leading us to conjecture that once H₂ has evolved from the hydrogenation surface of the palladium foil, the gas is likely not involved in the hydrogenation reaction and is therefore an undesired side product. Future catalyst designs may consider modifying the palladium membrane surface to hinder hydrogen recombination rates, thereby driving even higher current efficiencies.

Electrocatalytic palladium membrane reactors offer a compelling value proposition: electrolytic hydrogen driven through a palladium membrane can be used to hydrogenate organic molecules dissolved in any organic solvent without requiring an H₂ gas feedstock. We envision that this technology may be developed into a sustainable alternative to conventional high-temperature and high-pressure hydrogenation methods for fine chemical and industrial-scale applications. In this work, we move ePMRs toward this goal by providing a design for a scalable flow-reactor architecture and illuminating factors that define hydrogenation performance in these devices. We show that cell design considerations alone (i.e., improving mass transport of the organic feedstock to the palladium surface and increasing the maximum electrolysis current density) enable a 15-fold hydrogenation rate enhancement compared to the previously reported H-cell. We also conducted experiments that illustrate direct electrochemical control over the hydrogen content in the palladium membrane, which in turn mediates reaction rate and selectivity. We suggest that future studies focus on the reduction of more challenging substrates (e.g., carbonyls are harder to reduce than alkynes but are relevant for biofuel and pharmaceutical production) and the noble metal loading of the hydrogen-permeable membrane. We invite greater engagement from the materials science, chemistry, and engineering communities to realize the full potential of this nascent technology.

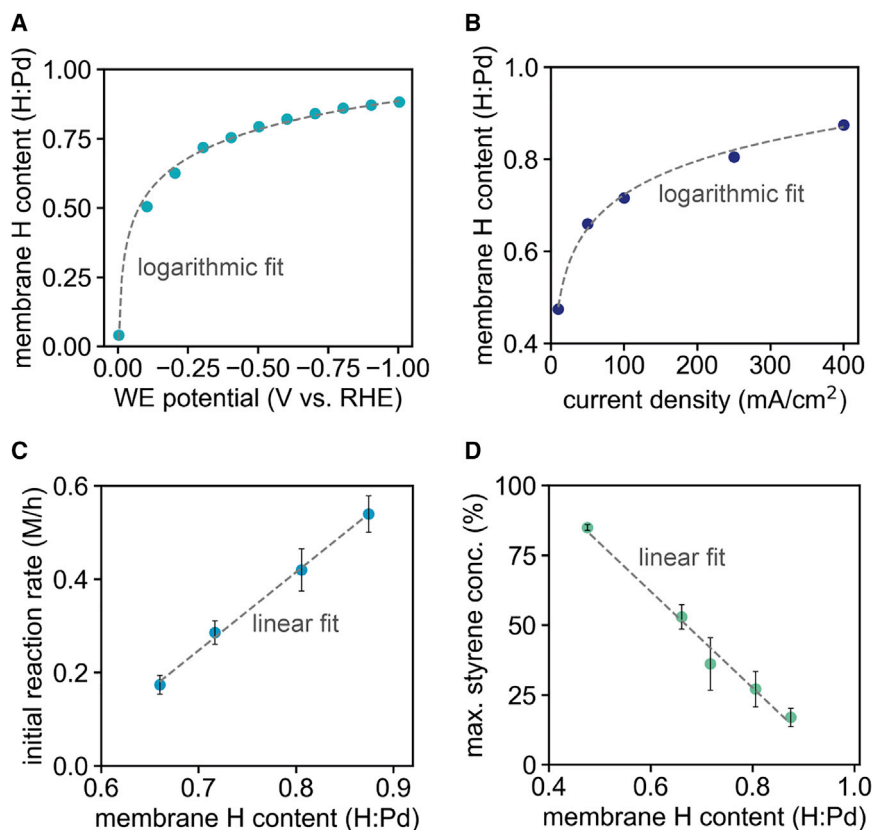


Figure 4. Hydrogen Content in the Palladium Membrane Affects Rate and Selectivity

(A and B) Plots illustrating the effect of (A) applied voltage and (B) current density on the amount of hydrogen that absorbs into the palladium membrane, showing direct electrochemical control over the palladium membrane hydrogen content (expressed as the H:Pd ratio).

(C and D) Plots showing that higher membrane hydrogen content (C) increases the initial reaction rate and (D) decreases selectivity for the styrene intermediate. Error bars represent ± 1 standard deviation of the mean value for at least 3 reactions.

EXPERIMENTAL PROCEDURES

Resource Availability

Lead Contact

Further information and requests for resources should be directed to the Lead Contact, Prof. Curtis P. Berlinguette (cberling@chem.ubc.ca).

Materials Availability

This study did not generate new unique reagents. Flow cell design details (including renderings and machine drawings) are freely available from the Lead Contact upon request.

Data and Code Availability

Raw datasets from hydrogenation experiments and kinetic model code are freely available from the Lead Contact upon request.

Procedure for Performing a Hydrogenation Experiment in an ePMR Flow Cell

To perform a hydrogenation reaction in the ePMR flow cell, the device was assembled by placing a palladium foil with the catalyst facing the hydrogenation flow field.

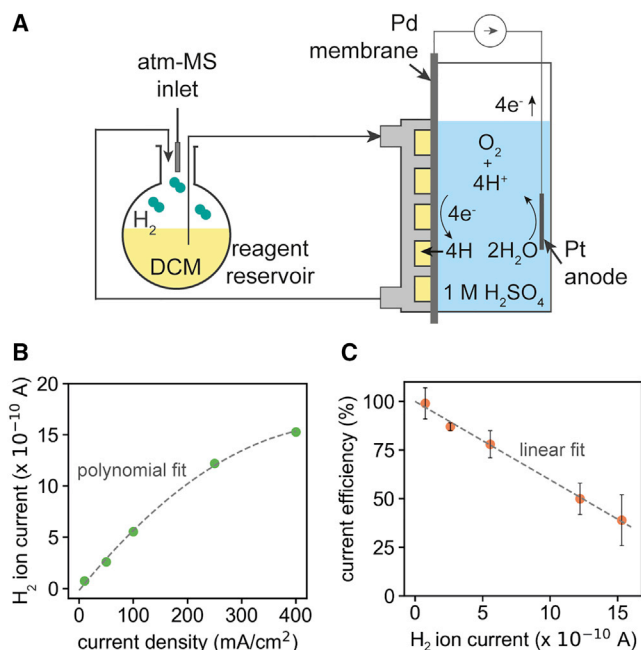


Figure 5. Hydrogen Permeation through the Palladium Membrane Affects CE

(A) Illustration of the experimental setup used to measure the amount of hydrogen that permeates through the palladium membrane by tracking the $m/z = 2$ ion current using *in situ* atmospheric pressure-mass spectrometry.

(B) The amount of hydrogen that permeates through the membrane increases with current density and is described by a polynomial fit.

(C) Plot showing that current efficiency decreases linearly with increasing hydrogen evolved at the side of the membrane where hydrogenation occurs. Error bars represent ± 1 standard deviation of the mean value for at least 3 experiments.

The compression plate, cathode chamber, Nafion membrane, and anode chamber were positioned over the foil. Four fasteners situated at the corners of the cell were tightened sequentially to compress the Viton Orings and create a hermetic seal between the component and component-membrane interfaces. Viton tubing ($1/8$ " inner diameter [ID], $1/4$ " outer diameter [OD]) was connected to the inlet and outlet of the hydrogenation flow plate via polyvinylidene difluoride (PVDF) Luer lock couplings, and connected the 50-mL organic reactant reservoir, peristaltic pump, and palladium membrane reactor. PA (0.26 g, 2.5 mmol) and DCM (25 mL) were added to the organic reagent reservoir and stirred at a consistent rate. Reaction aliquots were sampled every 1–30 min, depending on the current density and the duration of the reaction (e.g., 400 mA/cm² reactions were sampled approximately every 1 min for the first 5 samples, then every 10 min for the remaining samples, and 10 mA/cm² reactions were sampled approximately every 30 min from start to finish), such that 10–15 samples were collected for each reaction. Reactions were monitored by GC-MS by diluting 20 μ L of the reaction mixture in 1 mL DCM. See the [Supplemental Experimental Methods](#) for more details on palladium membrane fabrication, reaction characterization, kinetic modeling, and coulometry experiments.

SUPPLEMENTAL INFORMATION

Supplemental Information can be found online at <https://doi.org/10.1016/j.xcrp.2020.100105>.

ACKNOWLEDGMENTS

The authors are grateful to the Canadian Natural Science and Engineering Research Council (RGPIN-2018-06748 and STPGP-521255), the Canada Foundation for Innovation (229288), the Canadian Institute for Advanced Research (BSE-BERL-162173), and the Canada Research Chairs for financial support. This research was undertaken thanks in part to funding from the Canada First Research Excellence Fund, Quantum Materials and Future Technologies Program. We would like to acknowledge CMC Microsystems for the provision of products and services that facilitated this research, including SolidWorks. Finally, we thank Doug Yuen, Graham Liebelt, and Tobias Donaldson in the Department of Chemical and Biological Engineering at the University of British Columbia (UBC) for machining the custom apparatus presented in this work.

AUTHOR CONTRIBUTIONS

R.P.J., R.S.S., and C.P.B. designed the study. R.P.J., A.M.M., and A.K. performed the hydrogenation experiments. A.H. helped with the palladium membrane characterization. C.P.B. supervised the project. All of the authors contributed to the construction of the manuscript.

DECLARATION OF INTERESTS

The authors have submitted an international patent application related to the palladium membrane reactor (PCT/CA/2019/050097).

Received: March 30, 2020

Revised: May 4, 2020

Accepted: May 26, 2020

Published: July 8, 2020

REFERENCES

- Schiffer, Z.J., and Manthiram, K. (2017). Electrification and Decarbonization of the Chemical Industry. *Joule* 1, 10–14.
- Service, R. (2018). Liquid Sunshine. *Science* 361, 120–123.
- Weekes, D.M., Salvatore, D.A., Reyes, A., Huang, A., and Berlinguette, C.P. (2018). Electrolytic CO₂ Reduction in a Flow Cell. *Acc. Chem. Res.* 51, 910–918.
- Buttler, A., and Spliethoff, H. (2018). Current status of water electrolysis for energy storage, grid balancing and sector coupling via power-to-gas and power-to-liquids: a review. *Renew. Sustain. Energy Rev.* 82, 2440–2454.
- Bonrath, W., Medlock, J., Schutz, J., Wustenberg, B., and Netscher, T. (2012). Hydrogenation in the Vitamins and Fine Chemicals Industry – An Overview. In *Hydrogenation*, I. Karamé, ed. (IntechOpen). <https://doi.org/10.5772/48751>.
- Rylander, P.N. (1979). *Catalytic Hydrogenation in Organic Syntheses* (Academic Press).
- Jang, E.S., Jung, M.Y., and Min, D.B. (2005). Hydrogenation for Low Trans and High Conjugated Fatty Acids. *Compr. Rev. Food Sci. Food Saf.* 4, 22–30.
- Knothe, G. (2010). Biodiesel and renewable diesel: a comparison. *Pror. Energy Combust. Sci.* 36, 364–373.
- Sherbo, R.S., Kurimoto, A., Brown, C.M., and Berlinguette, C.P. (2019). Efficient Electrocatalytic Hydrogenation with a Palladium Membrane Reactor. *J. Am. Chem. Soc.* 141, 7815–7821.
- Delima, R.S., Sherbo, R.S., Dvorak, D.J., Kurimoto, A., and Berlinguette, C.P. (2019). Supported palladium membrane reactor architecture for electrocatalytic hydrogenation. *J. Mater. Chem. A* 7, 26586–26595.
- Sherbo, R.S., Delima, R.S., Chiykowski, V.A., MacLeod, B.P., and Berlinguette, C.P. (2018). Complete electron economy by pairing electrolysis with hydrogenation. *Nat. Catal.* 1, 501–507.
- Inoue, H., Abe, T., and Iwakura, C. (1996). Successive hydrogenation of styrene at a palladium sheet electrode combined with electrochemical supply of hydrogen. *Chem. Commun.* 0, 55–56.
- Iwakura, C., Yoshida, Y., and Inoue, H. (1997). A new hydrogenation system of 4-methylstyrene using a palladinized palladium sheet electrode. *J. Electroanal. Chem.* 431, 43–45.
- Wicke, E., Brodowsky, H., and Züchner, H. (1978). Hydrogen in palladium and palladium alloys. In *Hydrogen in Metals II: Application-Oriented Properties*, G. Alefeld and J. Völk, eds. (Springer), pp. 73–155.
- Dittmeyer, R., Höllein, V., and Daub, K. (2001). Membrane reactors for hydrogenation and dehydrogenation processes based on supported palladium. *J. Mol. Catal. Chem.* 173, 135–184.
- Maoka, T., and Enyo, M. (1981). Hydrogen absorption by palladium electrode polarized in sulfuric acid solution containing surface active substances—I. The cathodic region. *Electrochim. Acta* 26, 607–614.
- Yan, B., Bisbey, R.P., Alabugin, A., and Surendranath, Y. (2019). Mixed Electron-Proton Conductors Enable Spatial Separation of Bond Activation and Charge Transfer in Electrocatalysis. *J. Am. Chem. Soc.* 141, 11115–11122.
- Iwakura, C., Yoshida, Y., Ogata, S., and Inoue, H. (1998). New hydrogenation systems of unsaturated organic compounds using noble metal-deposited palladium sheet electrodes with three-dimensional structures. *J. Mater. Res.* 13, 821–824.
- Iwakura, C., Takezawa, S., and Inoue, H. (1998). Catalytic reduction of carbon dioxide with atomic hydrogen permeating through

- palladized Pd sheet electrodes. *J. Electroanal. Chem.* **459**, 167–169.
20. Iwakura, C., Ito, T., and Inoue, H. (1999). Construction of a new dehydrogenation system using a two-compartment cell separated by a palladized Pd sheet electrode. *J. Electroanal. Chem.* **463**, 116–118.
 21. Inoue, H., Higashiyama, K., Higuchi, E., and Iwakura, C. (2003). A dechlorination system for 4-chlorotoluene using a two-compartment cell separated by a palladized ion exchange membrane. *J. Electroanal. Chem.* **560**, 87–91.
 22. Sato, T., Takada, A., and Itoh, N. (2017). Low-temperature Hydrogenation of Toluene by Electrolysis of Water with Hydrogen Permeable Palladium Membrane Electrode. *Chem. Lett.* **46**, 477–480.
 23. Wang, J., Wang, H., and Fan, Y. (2018). Techno-Economic Challenges of Fuel Cell Commercialization. *Engineering*. **4**, 352–360.
 24. Plutschack, M.B., Pieber, B., Gilmore, K., and Seeberger, P.H. (2017). The Hitchhiker's Guide to Flow Chemistry. *Chem. Rev.* **117**, 11796–11893.
 25. Pletcher, D., Green, R.A., and Brown, R.C.D. (2018). Flow Electrolysis Cells for the Synthetic Organic Chemistry Laboratory. *Chem. Rev.* **118**, 4573–4591.
 26. Horiuti, I., and Polanyi, M. (1934). Exchange reactions of hydrogen on metallic catalysts. *Trans. Faraday Soc.* **30**, 1164–1172.
 27. Wilhite, B.A., McCreedy, M.J., and Varma, A. (2002). Kinetics of Phenylacetylene Hydrogenation over Pt/ γ -Al₂O₃ Catalyst. *Ind. Eng. Chem. Res.* **41**, 3345–3350.
 28. Mattson, B., Foster, W., Greimann, J., Hoette, T., Le, N., Mirich, A., Wankum, S., Cabri, A., Reichenbacher, C., and Schwanke, E. (2013). Heterogeneous Catalysis: The Horiuti–Polanyi Mechanism and Alkene Hydrogenation. *J. Chem. Educ.* **90**, 613–619.
 29. Studt, F., Abild-Pedersen, F., Bligaard, T., Sørensen, R.Z., Christensen, C.H., and Nørskov, J.K. (2008). Identification of non-precious metal alloy catalysts for selective hydrogenation of acetylene. *Science* **320**, 1320–1322.
 30. Al-Ammar, A.S., and Webb, G. (1978). Hydrogenation of acetylene over supported metal catalysts. Part 1.—Adsorption of [¹⁴C] acetylene and [¹⁴C] ethylene on silica supported rhodium, iridium and palladium and alumina supported palladium. *J. Chem. Soc. Faraday Trans.* **74**, 195–205.
 31. Sherbo, R.S., Moreno-Gonzalez, M., Johnson, N.J.J., Dvorak, D.J., Fork, D.K., and Berlinguette, C.P. (2018). Accurate Coulometric Quantification of Hydrogen Absorption in Palladium Nanoparticles and Thin Films. *Chem. Mater.* **30**, 3963–3970.
 32. Teschner, D., Borsodi, J., Wootsch, A., Révay, Z., Hävecker, M., Knop-Gericke, A., Jackson, S.D., and Schlögl, R. (2008). The roles of subsurface carbon and hydrogen in palladium-catalyzed alkyne hydrogenation. *Science* **320**, 86–89.
 33. Wilde, M., Fukutani, K., Ludwig, W., Brandt, B., Fischer, J.-H., Schauermaun, S., and Freund, H.-J. (2008). Influence of carbon deposition on the hydrogen distribution in Pd nanoparticles and their reactivity in olefin hydrogenation. *Angew. Chem. Int. Ed.* **47**, 9289–9293.
 34. Huang, D.C., Chang, K.H., Pong, W.F., Tseng, P.K., Hung, K.J., and Huang, W.F. (1998). Effect of Ag-promotion on Pd catalysts by XANES. *Catal. Lett.* **53**, 155–159.
 35. Khan, N.A., Shaikhutdinov, S., and Freund, H.-J. (2006). Acetylene and Ethylene Hydrogenation on Alumina Supported Pd-Ag Model Catalysts. *Catal. Lett.* **108**, 159–164.
 36. Ludwig, W., Savara, A., Brandt, B., and Schauermaun, S. (2011). A kinetic study on the conversion of cis-2-butene with deuterium on a Pd/Fe₃O₄ model catalyst. *Phys. Chem. Chem. Phys.* **13**, 966–977.
 37. Ludwig, W., Savara, A., Dostert, K.-H., and Schauermaun, S. (2011). Olefin hydrogenation on Pd model supported catalysts: new mechanistic insights. *J. Catal.* **284**, 148–156.
 38. Doyle, A.M., Shaikhutdinov, S.K., Jackson, S.D., and Freund, H.-J. (2003). Hydrogenation on metal surfaces: why are nanoparticles more active than single crystals? *Angew. Chem. Int. Ed.* **42**, 5240–5243.
 39. Daley, S.P., Utz, A.L., Trautman, T.R., and Ceyer, S.T. (1994). Ethylene Hydrogenation on Ni(111) by Bulk Hydrogen. *J. Am. Chem. Soc.* **116**, 6001–6002.

Cell Reports Physical Science, Volume 1

Supplemental Information

**Hydrogenation without H₂ Using
a Palladium Membrane Flow Cell**

Ryan P. Jansonius, Aiko Kurimoto, Antonio M. Marelli, Aoxue Huang, Rebecca S. Sherbo, and Curtis P. Berlinguette

Supplemental Experimental Methods

Materials

Pd (99.95%) was purchased as a 1 oz wafer bar from Silver Gold Bull. Phenylacetylene (98%) was purchased from Acros organics. Dichloromethane (DCM; obtained from a solvent purification system), H₂O₂ solution (30 wt. % in H₂O) were purchased from Sigma Aldrich. Pt gauze (52 mesh, 99.9%) and Pt wire (0.5 mm, 99.95%) were purchased from Alfa Aesar. Nitric acid (68-70%) was purchased from VWR. Nafion 117 membranes were purchased from Fuel Cell Store. Ag/AgCl reference electrodes (RE5B) were purchased from BASi. Cast PEEK sheets, borosilicate sheets, stainless steel dowel pins, stainless steel fasteners, and Viton o-rings and tubing and PVDF Luer lock quick connect tubing couplings for the fabrication of the flow cell were purchased from McMaster-Carr. The reaction mixture was pumped with a Low-Flow Chemical Metering Pump (part no. 4049K55, McMaster-Carr).

Pd foil preparation

Pd foils were rolled from a 1 oz Pd wafer bar. The bar was rolled to 25 μm thick foils as determined by a Mitutoyo digital micrometer and annealed at 850 °C for 1.5 hours in an Ar atmosphere. The Pd foils were cleaned using 1:1:1 conc. HNO₃:H₂O:H₂O₂ v/v ratio solution until vigorous bubbling subsided (~ 20 min). Electrodeposition was performed immediately following this cleaning step (see catalyst preparation below).

Electrochemistry

A Metrohm Autolab PGSTAT302N potentiostat was used to control the electrochemical experiments. A palladium foil was fitted between the hydrogenation flow field and the electrolysis

compartment. A Nafion 117 membrane (50- μm thick) was installed between the anode and cathode compartments. Viton o-rings were used to seal both the palladium foil and the Nafion membrane in place and ensure a reliable seal. Each electrolysis compartment was filled with 8 mL of 1 M H_2SO_4 , and an Ag/AgCl electrode (3.0 M NaCl) was used as a reference electrode and a Pt mesh was used as an anode/counter electrode. Electrolysis was driven galvanostatically, where a reductive current was applied by the potentiostat to the Pd foil working electrode (cathode) and the potential was measured between the Pd and the reference electrode. No iR correction was performed because the high salt concentration of the electrolyte and close proximity of the reference electrode to the palladium cathode (~ 3 mm) resulted in negligibly small uncompensated resistances of $<0.1 \Omega$. Cell potential (E_{cell}) was measured between the anode and cathode and is reported in this work as the absolute value for ease of comparison. The thickness of the foil was 25 μm and the geometric surface area of the foil was $\sim 9 \text{ cm}^2$.

Catalyst preparation

A high surface area palladium catalyst was electrodeposited onto the foil to increase the hydrogenation reaction rate. The cell was assembled without the cathode pressure plate installed, and with the side of the foil to which the organic substrate would be exposed during the reaction was instead exposed to the electrochemical compartment. The electrochemical chamber of the cell was filled with 15 mL of 15.9 mM PdCl_2 in 1 M HCl and a Ag/AgCl reference electrode and Pt mesh counter electrode were fitted to the cell. -0.3 V vs. Ag/AgCl was applied to the working electrode foil until 36 C of charge (9 C/cm^2) had been passed ($\sim 20 \text{ mg}$ of Pd). The deposition current was approximately 20–30 mA. The resulting black-coloured palladium catalyst was used for a maximum of 4 reactions before being removed from the foil using concentrated nitric acid and gentle mechanical abrasion. The foil was then

cleaned and replated with the catalyst for continued use. The palladium foils were used in this manner until pin holes formed in the foil as a result of: i) hydrogen embrittlement from repeated hydrogen absorption and desorption; ii) etching of the foil during cleaning; and iii) repeated clamping of the foil in the flow cell. The palladium membranes were reused for >10 reactions before pin-holes formed occurred.

Hydrogenation experiments in a flow cell

Please see the “Experimental Procedures” section in the main text for a detailed description of reaction setup and monitoring in the flow cell.

Hydrogenation experiments in an H-cell

Hydrogenation in H-cell was performed in air at room temperature. The oven-dried hydrogenation compartment with a magnetic stir bar was filled with substrate (2.5 mmol of phenylacetylene) and solvent (DCM, 25 mL). Electrolyte (1 M H₂SO₄, 35 mL) was added to each electrochemical compartment separated by a Nafion membrane. A constant current density of 100 mA/cm² was applied (vs. Ag/AgCl₂) for 8 h. Both the reaction mixture and electrolyte solution were stirred at a constant rate throughout the experiment. Reaction aliquots were sampled every 1 h to monitor the reaction progress by GC-MS.

Gas chromatography–mass spectrometry

GC–MS experiments were conducted on an Agilent GC–MS using an HP-5ms column and electron ionization. The samples were run using an auto-sampler with a 1 μL injection volume and a

split ratio of 20:1. The oven temperature was static at 50°C for 1 min, ramped to 65°C at 3 °C min⁻¹, then to 200°C at 100°C. A solvent delay of 4.6 min was employed. Peaks for phenylacetylene (PA), styrene (ST), and ethylbenzene (EB) were identified by searching the NIST database for matching mass spectra and eluted at 5.4, 5.8, and 5.1 minutes respectively. Relative concentration was determined using peak integration of the three fully-separated peaks. Calibration curves were collected for PA, ST, and EB, and the instrument response for each species was found to be identical within acceptable error ($\pm 1 \sigma$) of three repeats of each calibration curve. Therefore, no calibration factor was applied.

Atmospheric–mass spectrometry

The cell was set up identically as for membrane reactor hydrogenation experiments with a few minor modifications to enable monitoring of hydrogen evolution at both sides of the membrane: i) no phenylacetylene was added to the reagent reservoir; ii) the reference electrode was removed and replaced with an inlet connector for the ATM–mass spectrometer; and iii) the electrolysis was performed using a two-electrode setup (i.e., no reference electrode was used) given that the reference electrode port was used instead for gas sampling. Electrolyte (8 mL of 1 M H₂SO₄) was added to both electrochemical compartments with a Nafion membrane in between. Hydrogen evolution at the side of the membrane exposed to the organic solvent was monitored through a MS inlet tube connected to the reagent reservoir. The 2 m/z ion current was monitored using an ESS CatalySys atmospheric–mass spectrometer with a flow rate into the instrument of 10 mL min⁻¹. The reagent reservoir was stirred and DCM was pumped through the hydrogenation compartment of the cell throughout the experiment. Monitoring between the reagent reservoir and electrochemical compartment was switched every 5 s with a 3 s purge

to measure H₂ evolving at both sides of the membrane simultaneously in a single experiment. Once H₂ evolution had equilibrated.

Flow coulometry experiments

For the H:Pd measurements, a 3-step workflow was employed to collect each data point, using an electrochemical cell and protocol we have published previously.¹ First, a reductive potential between 0 and -1 V vs. RHE was applied to the electrode for 2000 s to drive hydrogen absorption into the palladium lattice. Next, 0.30 V (vs. Ag/AgCl) was applied for 1200 s, which oxidized hydrogen absorbed in the lattice back into protons, while the amount of charge passed during this step was measured. Lastly, the total current passed during this oxidation step was integrated to yield the total charge associated with the oxidation of adsorbed hydrogen.¹ All H:Pd absorption values were determined by converting the oxidative (desorption) charge to moles using Faraday's constant. The moles of palladium in the sample divided the absorbed moles of hydrogen. The moles of palladium were calculated from the dry mass of the palladium sample.

Kinetic modelling

To determine the reaction order in phenylacetylene and styrene, we fit the relative concentration versus time profiles with a system of ordinary differential equations for zero, first and second order reactions using a custom Python script (see Equations S1 to S9 below; Figures S10 to S14). The concentration profiles were fit following a time delay (denoted herein as 'permeation time'; Figure S21) from the start of electrolysis to when hydrogenation commences (Figure S22). The model output effective rate constants² (k') which were used in turn to calculate the concentration of each species in solution. The comparison of the conventional Horiuti-Polanyi mechanism and direct hydrogenation

mechanism (proposed here) was carried out by comparing the quality of the fits for a system of equations that included the direct pathway (Equations S13 to S15), to a system of equations that omitted the direct pathway (i.e., Horiuti-Polanyi mechanism; Equations S10 to S12).

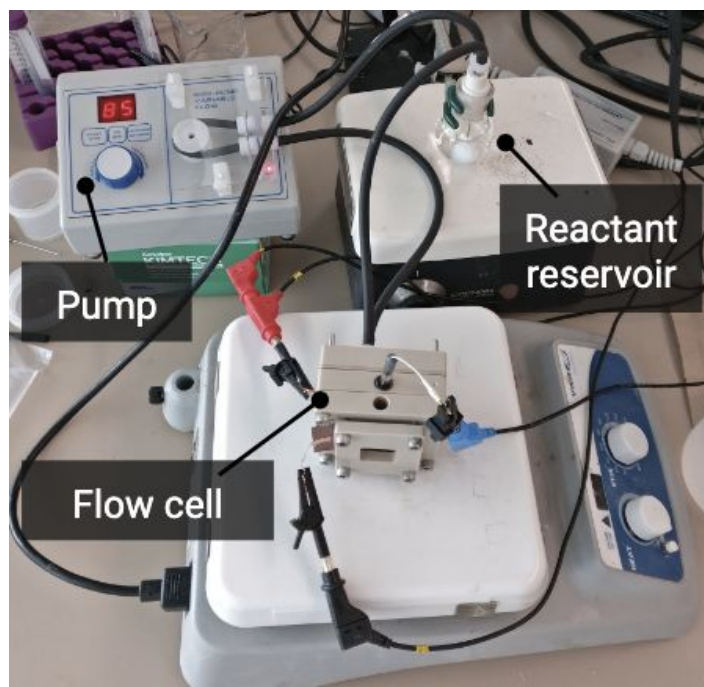


Figure S1. Labelled image of the functioning setup including the peristaltic pump, flow cell and reactant reservoir.

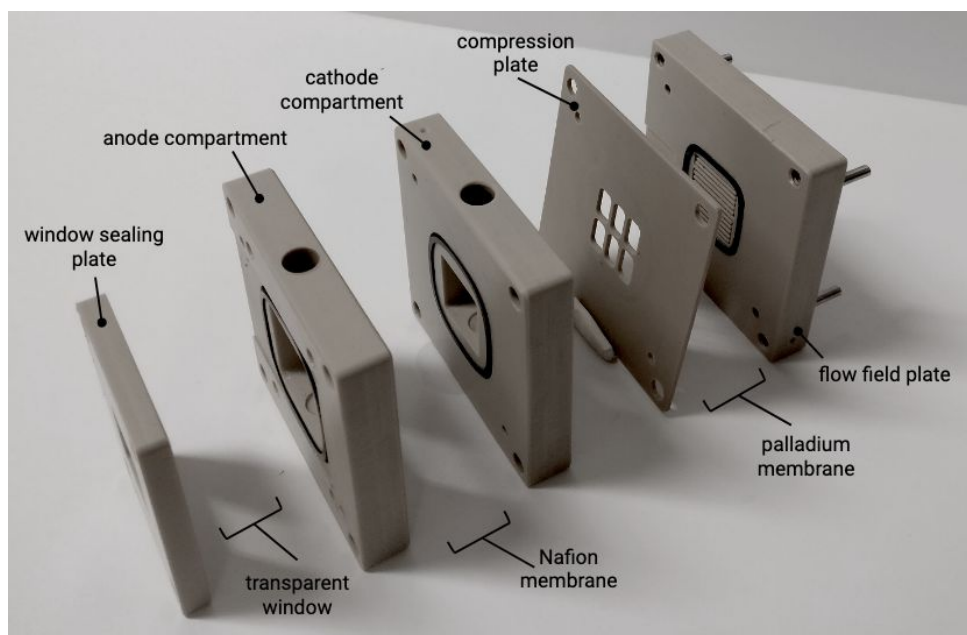


Figure S2. Labelled image of the electrocatalytic palladium membrane flow cell reported in this work

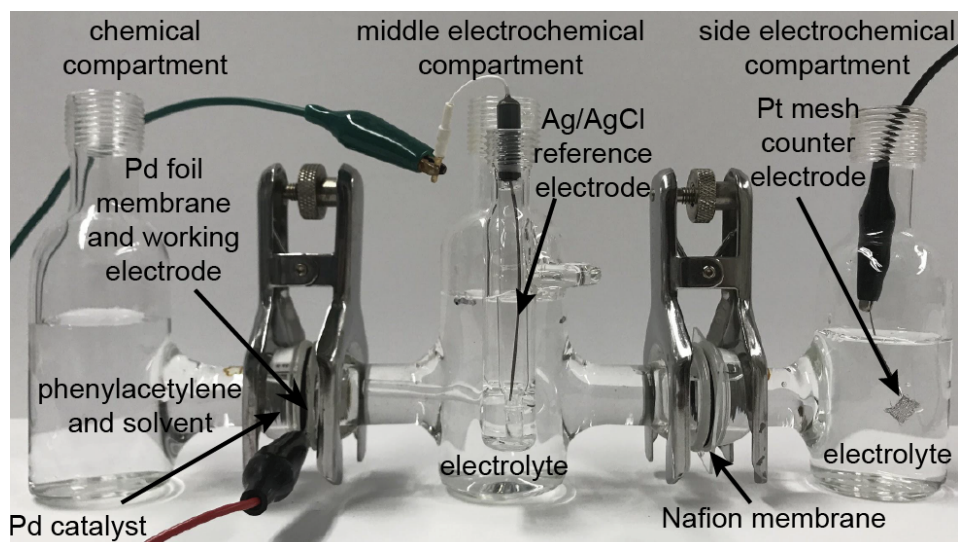


Figure S3. Labelled image of the electrocatalytic palladium membrane H-cell reported previously by our group.² Reprinted with permission from ref. 2. Copyright 2018 American Chemical Society.

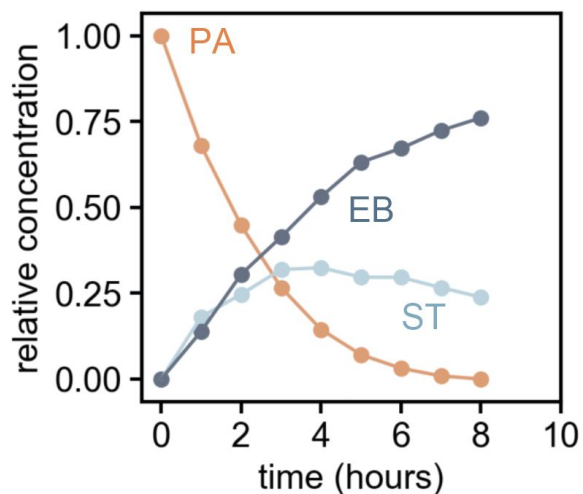


Figure S4. Concentration versus time plot for the hydrogenation of phenylacetylene in an ePMR H-cell. The phenylacetylene (PA) starting material was consumed after 8 hours of continuous electrolysis at 100 mA/cm^2 , producing styrene (ST) and ethylbenzene (EB).

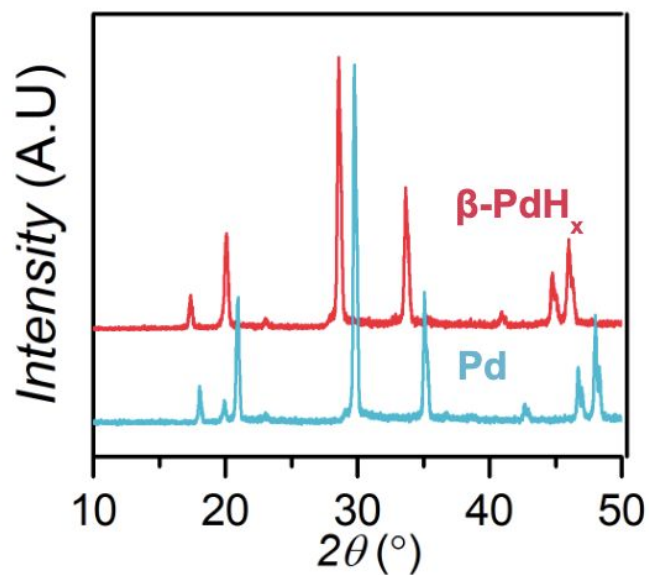


Figure S5. X-ray diffraction patterns of the as-prepared palladium membrane prior to electrolysis (Pd), and following electrolysis, during which the membrane absorbs hydrogen to form the hydride phase (β -PdH_x).

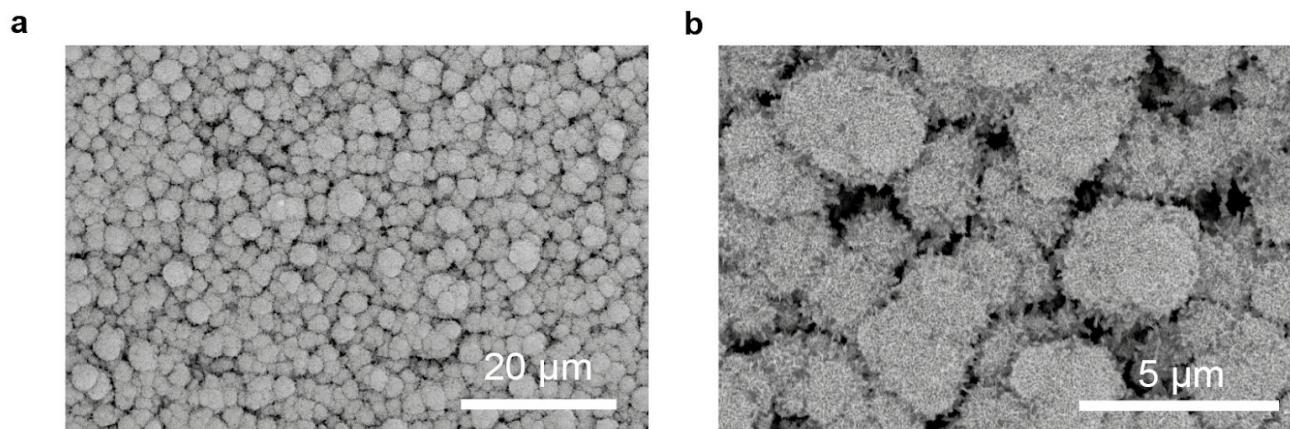


Figure S6. Scanning electron microscope images of the electrodeposited palladium electrocatalyst deposited on the hydrogenation surface of the palladium membrane at a magnification of; a) 2000, and b) 10000 times.

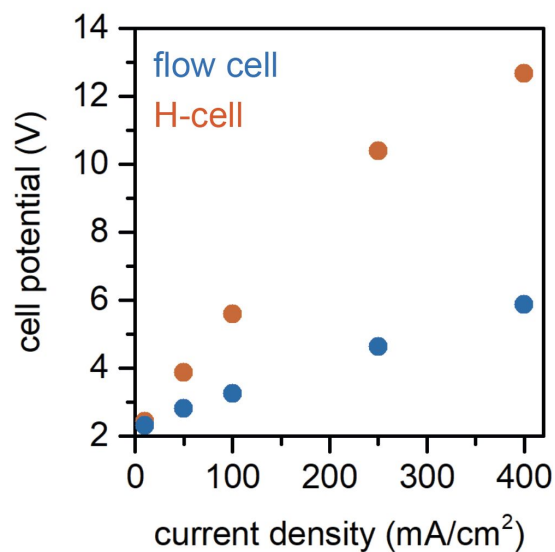


Figure S7. Plot of the cell voltage required to drive galvanostatic electrolysis at current densities between 10 and 400 mA/cm² in the previously reported H-cell and the novel flow cell presented in this work.

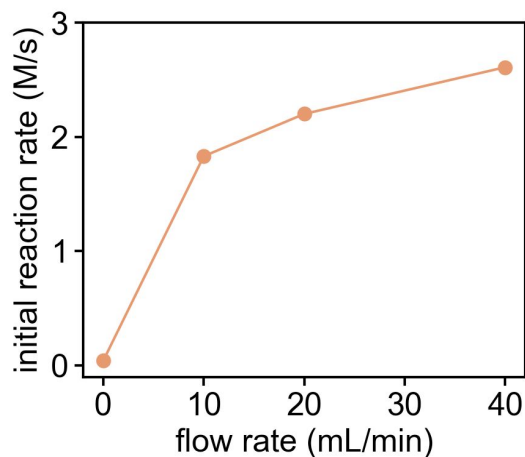


Figure S8. Plot showing the flow rate dependence of phenylacetylene hydrogenation rate in an ePMR at 100 mA/cm². The data point taken at 0 mL/min was collected in an H-cell. All other data points were collected using the ePMR flow cell presented in this work.

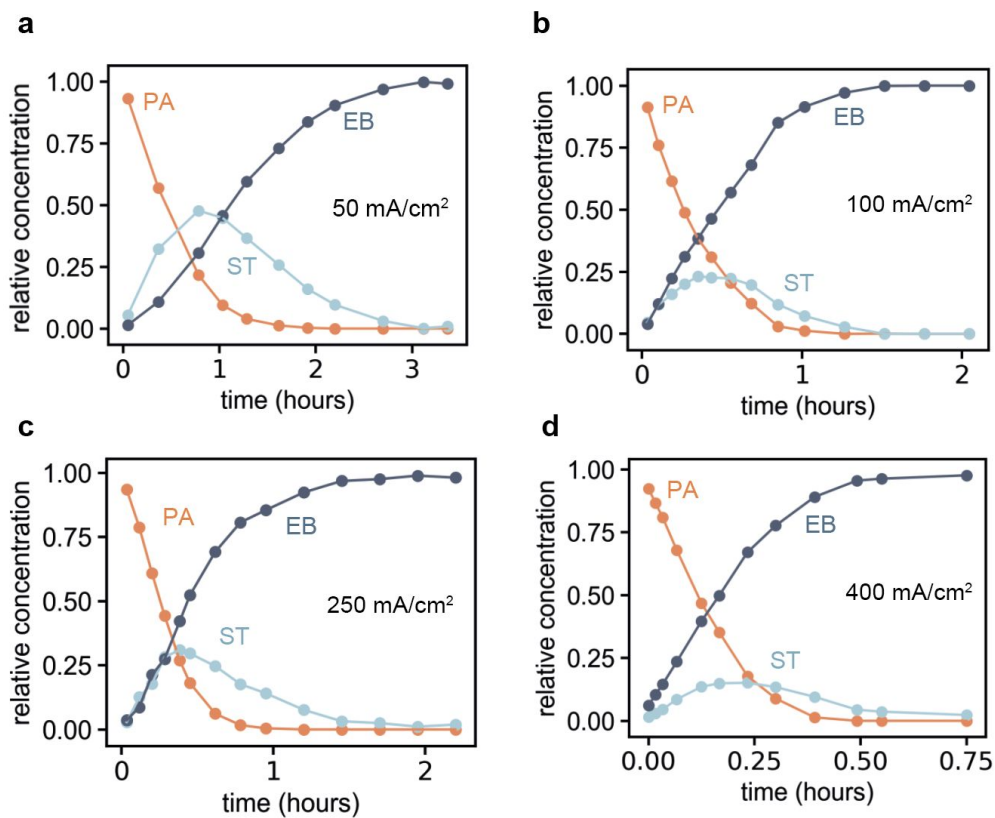


Figure S9. a) Plot of a reaction concentration profile for hydrogenation reactions carried out at a) 50 mA/cm² b) 100 mA/cm², c) 250 mA/cm² and d) 400 mA/cm². See Figure S16a for the 10 mA/cm² reaction profile.

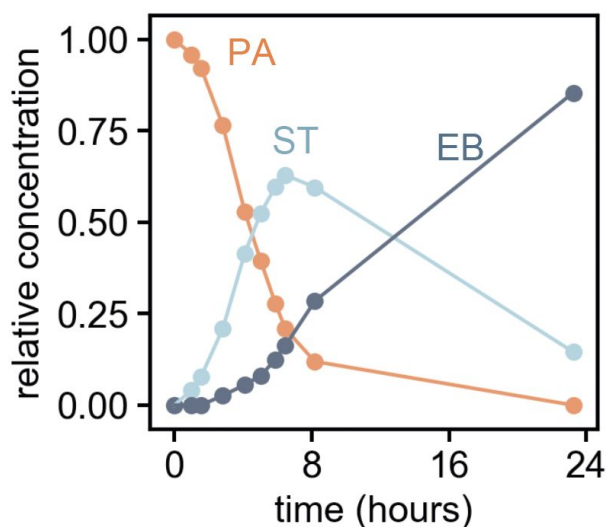
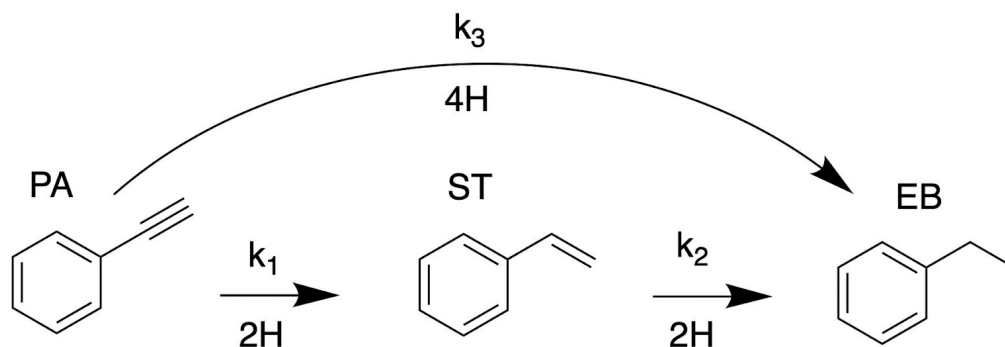


Figure 10. a) Plot of a reaction concentration profile for a 0.2 M, 200 mL solution of phenylacetylene, hydrogenated at 100 mA/cm².

Note S1. Kinetic modelling to determine phenylacetylene hydrogenation reaction order



Scheme S1. Hydrogenation scheme proposed here which includes a pathway for the direct hydrogenation of phenylacetylene to ethylbenzene. The conventional Horiuti-Polanyi mechanism omits the pathway for direct conversion of phenylacetylene to ethylbenzene (Scheme S2).³

System of equations for fitting the hydrogenation concentration profiles to **zero-order** reaction kinetics:

$$\frac{dPA}{dt} = -k_1[H]^x - k_3[H]^x = -k'_1 - k'_3 \quad [\text{Eq. S1}]$$

$$\frac{dST}{dt} = k_1[H]^x - k_2[H]^x = k'_1 - k'_2 \quad [\text{Eq. S2}]$$

$$\frac{dEB}{dt} = k_2[H]^x + k_3[H]^x = k'_2 + k'_3 \quad [\text{Eq. S3}]$$

System of equations for fitting the hydrogenation concentration profiles to **first-order** reaction kinetics:

$$\frac{dPA}{dt} = -k'_1[PA] - k'_3[PA] \quad [\text{Eq. S4}]$$

$$\frac{dST}{dt} = k'_1[PA] - k'_2[ST] \quad [\text{Eq. S5}]$$

$$\frac{dEB}{dt} = k'_2[ST] + k'_3[PA] \quad [\text{Eq. S6}]$$

System of equations for fitting the hydrogenation concentration profiles to **second-order** reaction kinetics:

$$\frac{dPA}{dt} = -k'_1[PA]^2 - k'_3[PA]^2 \quad [\text{Eq. S7}]$$

$$\frac{dS}{dt} = k'_1[PA]^2 - k'_2[ST]^2 \quad [\text{Eq. S8}]$$

$$\frac{dEB}{dt} = k'_2[ST]^2 + k'_3[PA]^2 \quad [\text{Eq. S9}]$$

Table S1. Comparison of goodness of fit for zero, first and second order reaction models (with respect to the organic reagent) for hydrogenation of phenylacetylene. The highest R^2 for each current density is highlighted with bold-faced text

Reaction conditions	Order determination		
	R^2 zero order	R^2 first order	R^2 second order
10 mA/cm ²	0.996	0.938	0.857
50 mA/cm ²	0.360	0.984	0.863
100 mA/cm ²	0.449	0.991	0.899
250 mA/cm ²	0.304	0.998	0.933
400 mA/cm ²	0.646	0.990	0.912

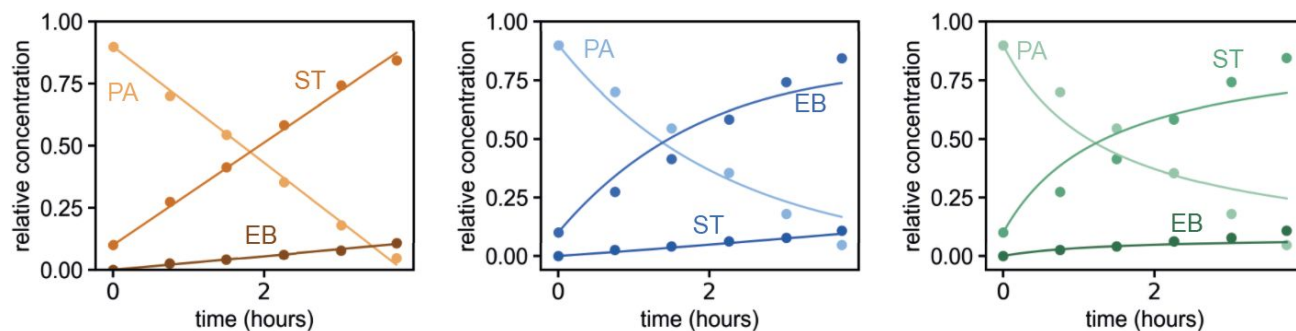


Figure S11. Comparison of fits for zero (orange), first (blue) and second (green) order reaction models to determine fit for hydrogenation when **10 mA/cm²** of electrolysis current was applied. Only the first 4 hours of the reaction were fit to each model to simplify the visual comparison. The 0-order equations (orange) provide the best fit.

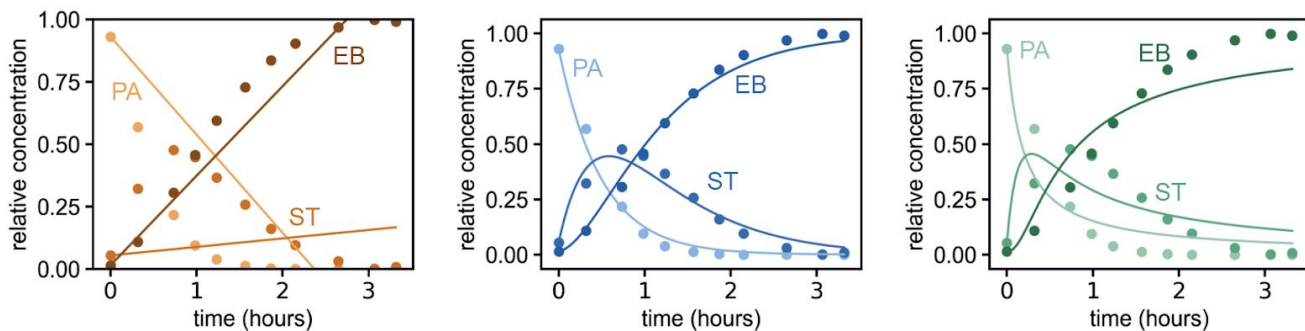


Figure S12. Comparison of fits for zero (orange), first (blue) and second (green) order reaction models to determine fit for hydrogenation when 50 mA/cm^2 of electrolysis current was applied. The 1st-order equations provide the best fit.

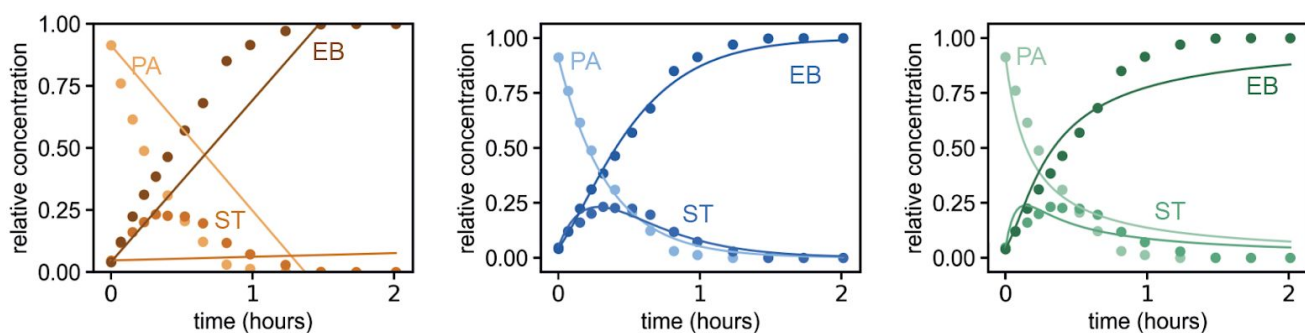


Figure S13. Comparison of fits for zero (orange), first (blue) and second (green) order reaction models to determine fit for hydrogenation when 100 mA/cm^2 of electrolysis current was applied. The 1st-order equations provide the best fit.

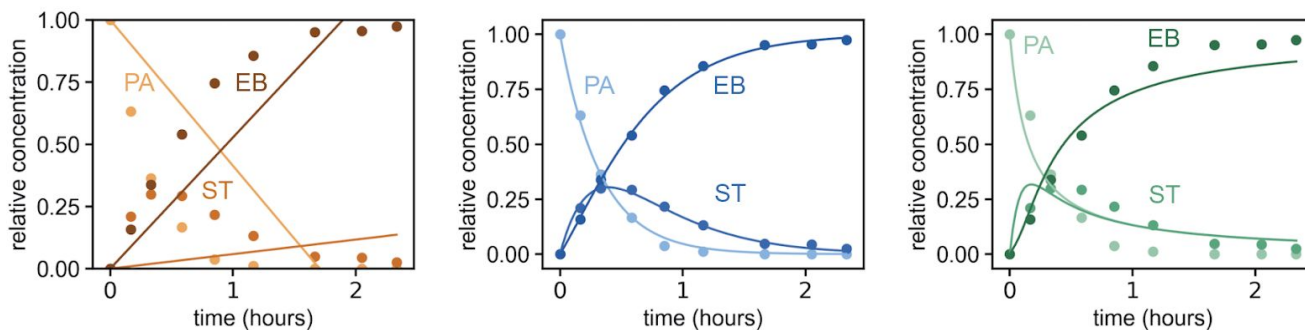


Figure S14. Comparison of fits for zero (orange), first (blue) and second (green) order reaction models to determine fit for hydrogenation when 250 mA/cm^2 of electrolysis current was applied. The 1st-order equations provide the best fit.

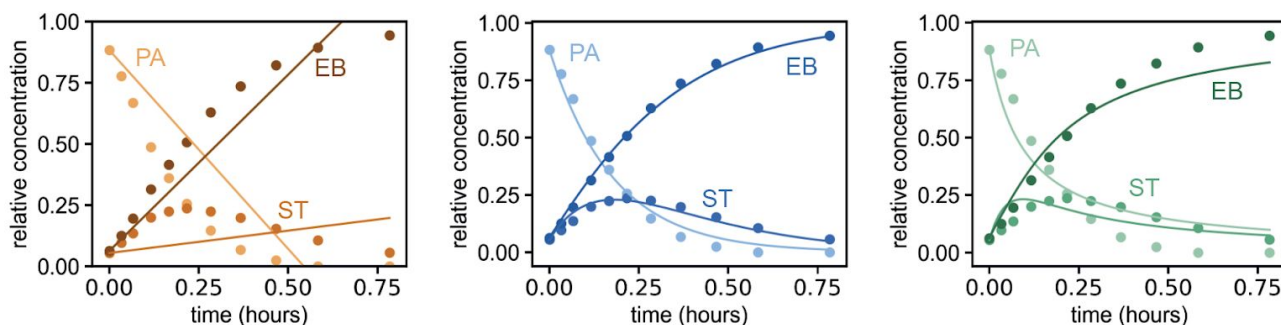
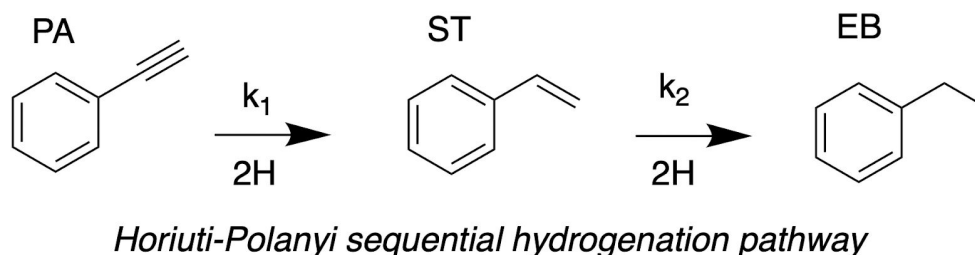


Figure S15. Comparison of fits for zero (orange), first (blue) and second (green) order reaction models to determine fit for hydrogenation when 400 mA/cm^2 of electrolysis current was applied. The 1st-order equations provide the best fit.

Note S2. Comparison of hydrogenation mechanisms

Scheme S2. Hydrogenation scheme consistent with the well-established Horiuti-Polanyi mechanism⁴



System of equations for fits using a **sequential** hydrogenation mechanism, in line with the conventional Horiuti-Polanyi mechanism (Scheme S2):

$$\frac{dPA}{dt} = -k_1[H]^x[PA] = -k'_1[PA] \quad [\text{Eq. S10}]$$

$$\frac{dST}{dt} = k_1[H]^x[PA] - k_2[H]^x[ST] = k'_1[PA] - k'_2[ST] \quad [\text{Eq. S11}]$$

$$\frac{dEB}{dt} = k_2[H]^x[ST] = k'_2[ST] \quad [\text{Eq. S12}]$$

System of equations for fits which includes both the sequential, and also **direct** hydrogenation pathways (Scheme S1):

$$\frac{dPA}{dt} = -k'_1[PA] - k'_3[PA] \quad [\text{Eq. S13}]$$

$$\frac{dST}{dt} = k'_1[PA] - k'_2[ST] \quad [\text{Eq. S14}]$$

$$\frac{dEB}{dt} = k'_2[ST] + k'_3[PA] \quad [\text{Eq. S15}]$$

Table S2. Comparison of goodness of fit comparison for the direct and sequential reaction models for phenylacetylene hydrogenation

Reaction conditions	Order determination	
	R ² sequential model	R ² direct model
50 mA/cm ²	0.975	0.980
100 mA/cm ²	0.986	0.990
250 mA/cm ²	0.987	0.997
400 mA/cm ²	0.975	0.990

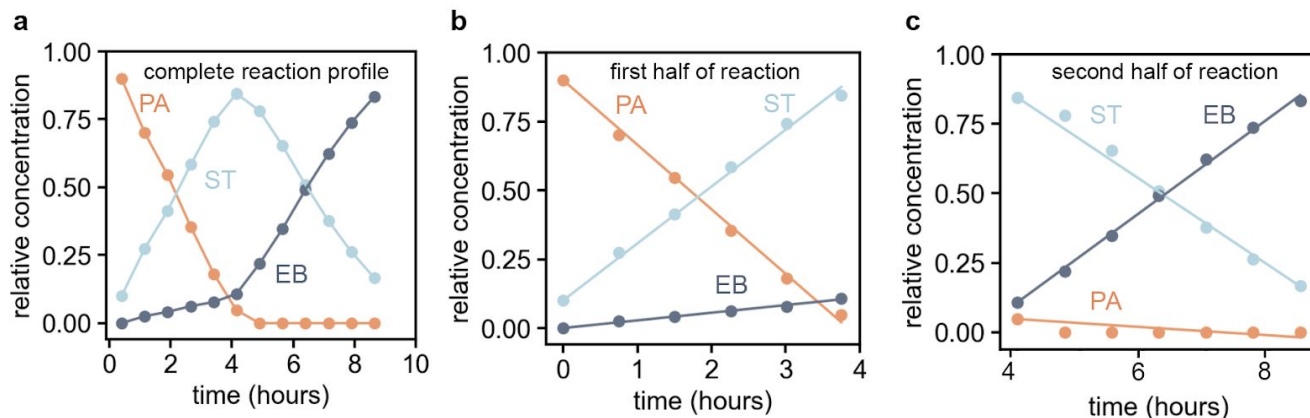


Figure S16. a) Plot of the complete reaction profile for phenylacetylene hydrogenation conducted at 10 mA/cm². The first and second 4-hour increments of the reaction were fit to the 0-order kinetic model separately (panels b and c, respectively) to identify the effective rate constants. b) We assume ethylbenzene formation during the first 4 hours of the reaction to correspond to the direct hydrogenation of phenylacetylene to ethylbenzene (see discussion section). The k_3' value was calculated based on this assumption. c) We take ethylbenzene formation during the final 4 hours of the reaction (when there is no phenylacetylene present) to correspond to hydrogenation of styrene to ethylbenzene and calculate k_2' based on this assumption.

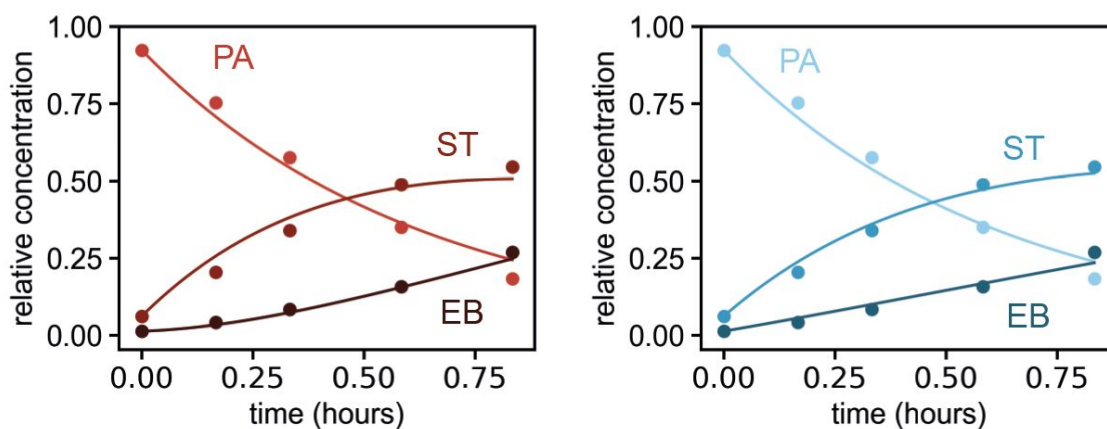


Figure S17. Comparison of the fits using the previously reported sequential hydrogenation pathway (red) and the proposed direct hydrogenation pathway (blue) for the hydrogenation of phenylacetylene under 50 mA/cm² electrolysis current. The best fit was provided by the system of equations that included a direct hydrogenation pathway.

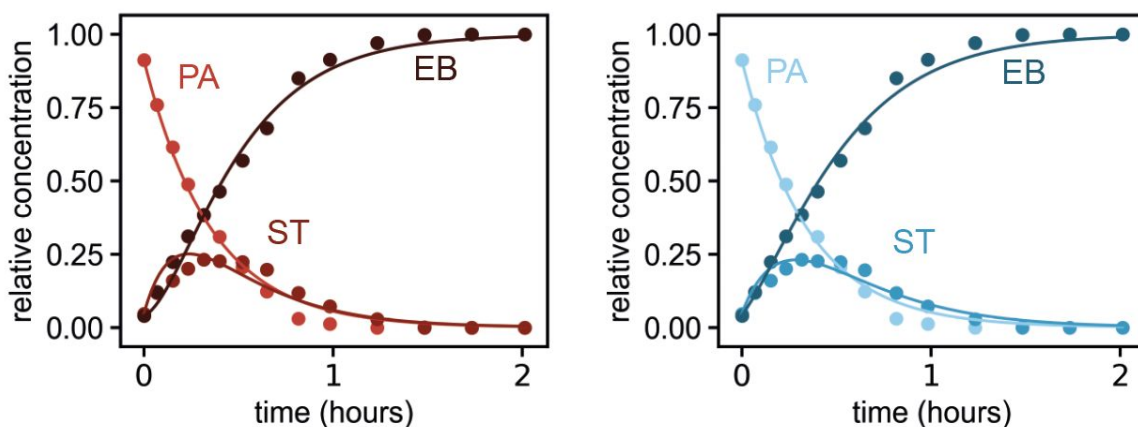


Figure S18. Comparison of the fits using the previously reported sequential hydrogenation pathway (red) and the proposed direct hydrogenation pathway (blue) for the hydrogenation of phenylacetylene under 100 mA/cm^2 electrolysis current. The best fit was provided by the system of equations that included a direct hydrogenation pathway.

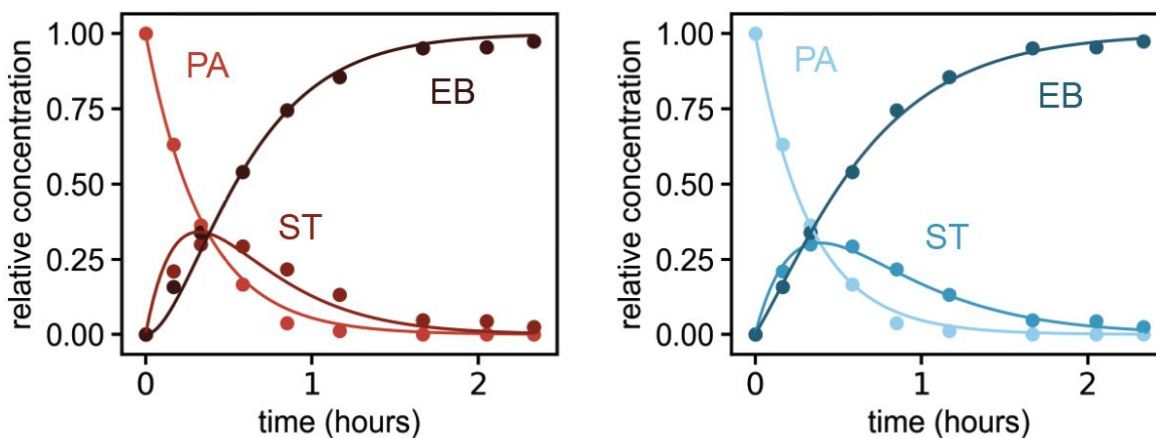


Figure S19. Comparison of the fits using the previously reported sequential hydrogenation pathway (red) and the proposed direct hydrogenation pathway (blue) for the hydrogenation of phenylacetylene under 250 mA/cm^2 electrolysis current. The best fit was provided by the system of equations that included a direct hydrogenation pathway.

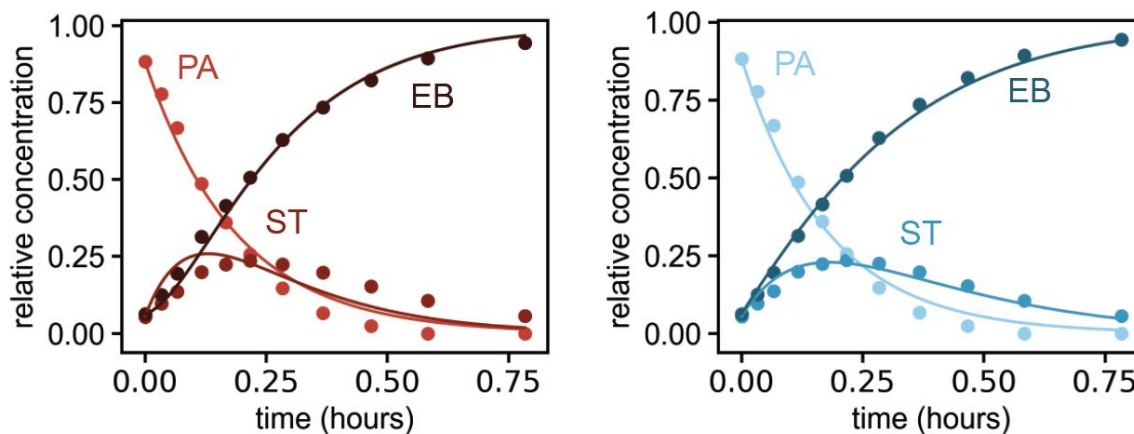


Figure S20. Comparison of the fits using the previously reported sequential hydrogenation pathway (red) and the proposed direct hydrogenation pathway (blue) for the hydrogenation of phenylacetylene under 400 mA/cm^2 electrolysis current. The best fit was provided by the system of equations that included a direct hydrogenation pathway.

Table S3. Effective rate constants calculated using a kinetic model for the hydrogenation reaction (Scheme S1) carried out at each current densities between 10 and 400 mA/cm^2

Reaction conditions	Effective rate constant (k') ^a		
	k_1'	k_2'	k_3'
Current density			
10 mA/cm^2	0.261 ± 0.025^1	0.003 ± 0.029	0.029 ± 0.011
50 mA/cm^2	1.500 ± 0.093	1.398 ± 0.240	0.145 ± 0.109
100 mA/cm^2	2.213 ± 0.239	2.378 ± 0.505	0.848 ± 0.009
250 mA/cm^2	2.253 ± 0.214	2.871 ± 1.278	1.182 ± 0.008
400 mA/cm^2	2.987 ± 0.446	5.856 ± 3.162	2.332 ± 0.496

^aNote that the units for the effective rate constants for the 10 mA/cm^2 reaction are M^2/s , and the units for the reactions carried out at $50\text{-}400 \text{ mA/cm}^2$ are M/s .

Equation used to calculate the initial rate of phenylacetylene consumption using effective rate constants in Table S3.

$$Rate_{initial} = (k_1' + k_3') \times [PA]_{initial} \quad [\text{Eq. S16}]$$

Equations used to calculate the current efficiency (CE) of the hydrogenation reaction. Where: *volume* is the total volume of reactant solution used (25 mL in most cases); i_{total} is the current density multiplied by the geometric size of the Pd membrane; Δt is the time elapsed between data points, and ; F is Faraday's constant.

$$CE (\%) = (\text{moles of } H \text{ consumed} / \text{moles of } H \text{ produced}) \times 100\% \quad [\text{Eq. S17}]$$

$$\text{moles of } H \text{ consumed} = (2 \times \Delta[ST] + 4 \times \Delta[EB]) \times \text{volume} \quad [\text{Eq. S18}]$$

$$\text{moles of } H \text{ produced} = (i_{total} \times \Delta t) / F \quad [\text{Eq. S19}]$$

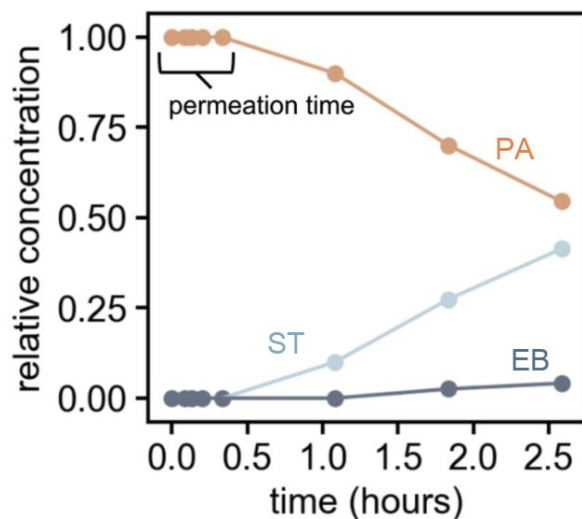


Figure S21. Tutorial plot showing a reaction concentration profile with the hydrogen permeation time annotated (which we define as the amount of time elapsed from the start of electrolysis to the first observation of hydrogenated products). See Figure S16a for the complete concentration profile for this reaction.

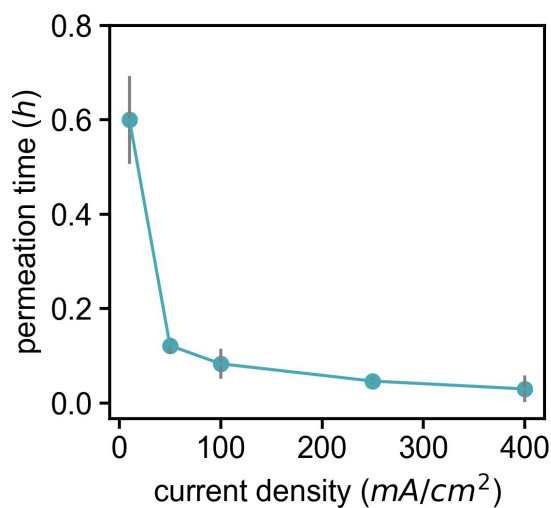


Figure S22. Plot showing that permeation time decreases exponentially with increasing current density. Error bars represent ± 1 standard deviation of the mean value for at least 3 reactions.

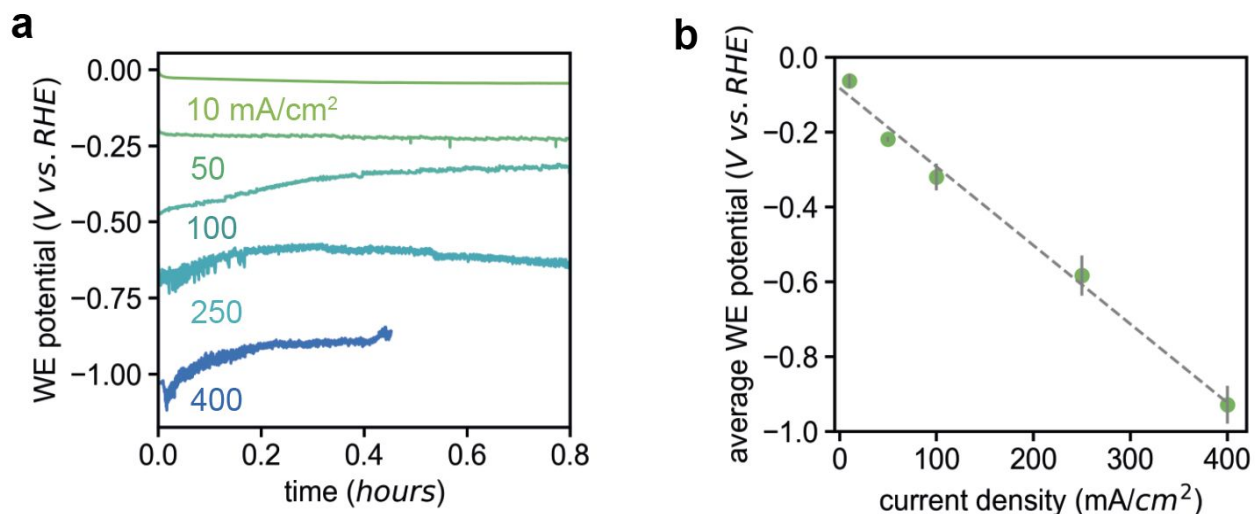


Figure S23. a) Overlay of chronopotentiometry traces for each electrolysis current density used in this study. The increase in the WE potential during electrolysis is likely due to hydrogen absorption into the palladium membrane to form β -PdH_x, which exhibits higher HER activity than Pd.⁵ b) Plot of the average potential (vs. RHE) required to mediate electrolysis at each current density. Error bars represent ± 1 standard deviation of the average potential used to drive the galvanostatic electrolysis in panel (a).

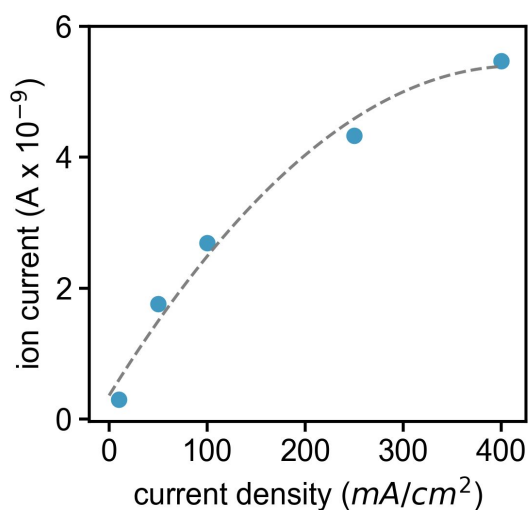


Figure S24. The amount of the hydrogen that evolves from the Pd membrane surface in the electrochemical chamber as current density increases is described by a 2nd order polynomial fit ($R^2 = 0.99$).

Equation describing the relationship between the amount of hydrogen absorbed into the palladium membrane as a function of applied potential (vs. RHE).

$$y = 0.185 \ln|x| + 0.907 \quad [\text{S20}]$$

References

1. Sherbo, R.S., Moreno-Gonzalez, M., Johnson, N.J.J., Dvorak, D.J., Fork, D.K., and Berlinguette, C.P. (2018). Accurate Coulometric Quantification of Hydrogen Absorption in Palladium Nanoparticles and Thin Films. *Chem. Mater.* *30*, 3963–3970.
2. Sherbo, R.S., Kurimoto, A., Brown, C.M., and Berlinguette, C.P. (2019). Efficient Electrocatalytic Hydrogenation with a Palladium Membrane Reactor. *J. Am. Chem. Soc.*, 7815–7821.
3. Horiuti, I., and Polanyi, M. (1934). Exchange reactions of hydrogen on metallic catalysts. *Trans. Faraday Soc.* *30*, 1164–1172.
4. Mattson, B., Foster, W., Greimann, J., Hoette, T., Le, N., Mirich, A., Wankum, S., Cabri, A., Reichenbacher, C., and Schwanke, E. (2013). Heterogeneous Catalysis: The Horiuti–Polanyi Mechanism and Alkene Hydrogenation. *J. Chem. Educ.* *90*, 613–619.
5. Sarkar, S., and Peter, S.C. (2018). An overview on Pd-based electrocatalysts for the hydrogen evolution reaction. *Inorg. Chem. Front.* *5*, 2060–2080.